Exact Coherent States

Fabian Waleffe, Notes by Chao Ma and Samuel Potter
Revised by FW

WHOI GFD Lecture 6, June 27, 2011

Abstract

Shear enhanced dissipation, $R^{1/3}$ scaling in shear flows. Critical layer in lower branch exact coherent states. SSP model modified to include critical layers. Construction of *exact coherent states* in full Navier-Stokes. Optimum traveling wave and near-wall coherent structures, 100+ streak spacing. Physical space structures of turbulence. State space structure of turbulence.

1 Shear enhanced dissipation

In the (quick) overview of the SSP model, we discussed how the shearing of x-dependent modes by the mean shear leads to a *positive* feedback on the mean flow. In the SSP model these are the W^2 term in the M equation and the $-MW$ term in the W equation. Although this interaction is not necessary for the self-sustaining process itself, it is the key effect that leads to the R^{-1} scaling of the transition threshold, and of the V and W components of the lower branch steady state (while U and $1-M$ are $O(1)$, see lectures 1 and 5).

Advection by a shear flow leads to enhanced dissipation and an $R^{-1/3}$ scaling characteristic of *linear* perturbations about shear flows, or evolution of a passive scalar. The $R^{-1/3}$ enhanced damping, instead of R^{-1}, was included by Chapman for the x-dependent modes in his modification of the WKH model (as discussed in lecture 1). However, that is because Chapman considers the weak nonlinear interaction of eigenmodes of the *laminar flow*, $U(y)$. In contrast, the basic description of the SSP consists of the weak nonlinear interaction of *streaky flow eigenmodes*, that is, neutral eigenmodes of the spanwise varying shear flow $U(y,z)$ consisting of the mean shear *plus* the streaks. An important aspect of the streaky flow $U(y,z)$ is that the mean shear has been reduced precisely to allow that instability, as illustrated by the SSP model where $\sigma_w U - \sigma_m M - \sigma_v V > 0$ is needed for streak instability and growth of W. So it is unclear *a priori* whether the $R^{-1/3}$ should apply to x-dependent modes in the SSP. In section 2 below we review the numerical evidence that the 3D nonlinear lower branch SSP states in plane Couette flow do have $R^{-1/3}$ critical layers as $R \to \infty$ [24]. But why $R^{1/3}$?

Back-of-the-envelope analysis. Consider plane channel flow with near-wall velocity profile $U(y) \simeq Sy$ (Figure 1), where S is the shear rate. Denote $\hat{\mathbf{x}}$ as the flow direction and $\hat{\mathbf{y}}$ as the shear direction. We introduce a small disturbance which we imagine as a little eddy with characteristic length ℓ_0, generated perhaps using a push-pull perturbation as in some of the experiments of Mullin *et al.* discussed in lecture 1 with the push-pull axis oriented streamwise (we consider only 2D flow here). We assume that the eddy Reynolds number is small so that the evolution of the eddy consists primarily of

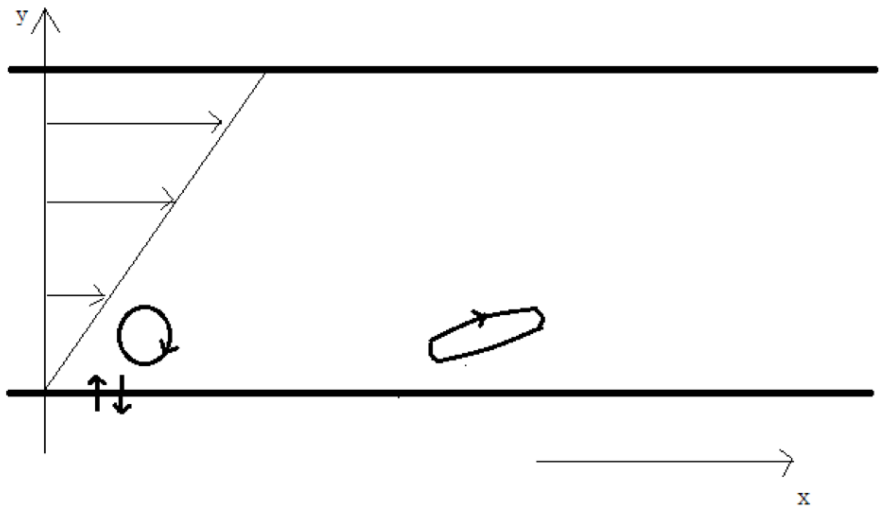

Figure 1: Shearing leads to enhanced dissipation and $R^{1/3}$ scaling.

the distortion by the mean shear (so small eddy Reynolds number and 2D means none of the Theodorsen horseshoes discussed in lecture 1), that is the governing equation is the advection diffusion of spanwise vorticity $\omega = \partial_x v - \partial_y u$

$$(\partial_t + Sy\,\partial_x - \nu\nabla^2)\,\omega = 0. \tag{1}$$

The eddy will be stretched in the $\hat{\mathbf{x}}$ direction as a result of the differential advection,[1] and the major axis a of this now elliptical eddy will grow like $a \sim \ell_0\sqrt{1+(St)^2} \sim \ell_0 St$, while its minor axis b will decay like $b \sim \ell_0^2/a \sim \ell_0/(St)$, since area is conserved in this 2D incompressible flow. This is the back-of-the-envelope handling of the $Sy\partial_x$ term in (1) and we now estimate the dissipation $\nu\nabla^2 \sim -\nu/\ell^2$ where the relevant length scale ℓ here is the *smallest scale* which is $b \sim \ell_0/(St)$ for long times. So the diffusion term will give

$$\frac{d\omega}{dt} \sim -\nu\frac{(St)^2}{\ell_0^2}\,\omega \quad \Rightarrow \quad \omega \sim \omega_0\,\exp\left(-\nu\frac{S^2t^3}{3\ell_0^2}\right) \tag{2}$$

Note that we have used a d/dt instead of ∂_t since we have taken care of the advection and are effectively doing a Lagrangian analysis. In the absence of differential advection, we would have $\omega \sim \omega_0\exp(-\nu St/\ell_0^2)$, so (2) is much smaller for $St > 3$, and differential advection leads to enhanced diffusion. In non-dimensional form, we can define a Reynolds number $R_0 = S\ell_0^2/\nu$ based on the length scale ℓ_0 and the velocity scale $S\ell_0$ and write (2) as

$$\frac{\omega}{\omega_0} \sim \exp\left(-\frac{(St)^3}{3R_0}\right) \tag{3}$$

where St is a nondimensional time based on the shear rate S and this shows that enhanced dissipation occurs on a time scale $St \sim R_0^{1/3}$. If we have a length scale, say h for the shear flow, then we can define a Reynolds number $R = Sh^2/\nu$ then $R_0 = R\,(\ell_0/h)^2$ and the enhanced dissipation occurs on the time scale $St \sim R^{1/3}(\ell_0/h)^{2/3}$, still scaling like $R^{1/3}$.

[1] Two material points at the same y do not separate, but two material points at the same x but ℓ_0 apart in y are differentially advected in x and the distance between them will be $\ell = \ell_0\sqrt{1+(St)^2}$.

Didn't he say 'analysis'? Fellows uncomfortable with the back of an envelope should go with the flow $x = x_0 - Syt$ and consider $\omega = \omega(x_0, y, t)$ in terms of the Lagrangian coordinate $x_0 = x + Syt$ and y, t, then $(\partial/\partial x)_{y,t} = (\partial/\partial x_0)_{y,t}$ but

$$(\partial/\partial y)_{x,t} = (\partial/\partial y)_{x_0,t} - \ St\ (\partial/\partial x_0)_{y,t} \tag{4}$$

$$(\partial/\partial t)_{x,y} = (\partial/\partial t)_{x_0,y} - \ Sy\ (\partial/\partial x_0)_{y,t} \tag{5}$$

and (1) for $\omega(x_0, y, t)$ becomes

$$\frac{\partial \omega}{\partial t} = \nu\big(1 + (St)^2\big)\,\frac{\partial^2 \omega}{\partial x_0^2} - 2\nu St\,\frac{\partial^2 \omega}{\partial x_0 \partial y} + \nu \frac{\partial^2 \omega}{\partial y^2} \tag{6}$$

that has solutions of the form $\omega = A(t) e^{i(\alpha x_0 + \beta_0 y)}$ with

$$A(t) = A_0 \exp\Big(-\nu \big((\alpha^2 + \beta_0^2)t - \alpha\beta_0 S t^2 + \alpha^2 S^2 t^3/3\big)\Big), \tag{7}$$

which for $\alpha = 1/\ell_0$, $\beta_0 = 0$ gives

$$\omega = \omega_0 \exp\left(-\nu\,\frac{t + S^2 t^3/3}{\ell_0^2}\right), \tag{8}$$

that should reassure fellows of the validity of (2).

One can also use *Kelvin modes* and solve (1) (in an infinite domain in y) using solutions of the form $\omega = A(t)\exp(i\mathbf{k}(t)\cdot\mathbf{r})$, that is, Fourier modes with time-dependent wavevectors $\mathbf{k}(t)$. For (1), one finds $\mathbf{k}(t) = (\alpha, \beta_0 - \alpha St)$ and $dA/dt = -\nu k^2 A$ with $k^2 = \alpha^2 + (\beta_0 - \alpha St)^2$ and recover (7). Thus, shearing leads to wavenumbers that grow like St in the shear direction $\beta \sim -\alpha St$ or $k_y \sim -k_x St$ and this leads to enhanced damping.

In a *semi-infinite* domain, *e.g.* $0 \le y < \infty$, the advection diffusion equation (1)[2] has eigensolutions of the form $e^{\lambda t} e^{i\alpha x} f(y)$ where $f(y)$ can be expressed in terms of Airy functions with y length scales $\sim (\nu/(\alpha S))^{1/3}$ and $\Re(\lambda) \sim -(\nu\alpha^2 S^2)^{1/3}$. For a *bounded domain*, the eigenmodes have y scale $\sim (\alpha R)^{-1/3}$ and decay rates $\sim (\alpha R)^{-1/3}$, with α now the non-dimensionalized x wavenumber. The connection between the y scale and the decay rate follows from the form of the dissipation $\partial_t = \nu\nabla^2 \sim -\nu k^2$ where k is a wavenumber. In non-dimensional units, this is $\partial_t \sim -k^2/R$ with $k \sim R^{1/3}$ for scales $\sim R^{-1/3}$, thus

$$-\frac{k^2}{R} \sim -R^{-1/3}. \tag{9}$$

2 $R^{-1/3}$ in lower branch exact coherent states

Lower branch exact coherent states, that is the unstable 3D steady states calculated from the Navier-Stokes equations using Newton's method and the SSP phenomenology [18], show $R^{-1/3}$ critical layers as illustrated by the plane Couette flow steady states in [24]. Those calculations (up to about $R \approx 60\,000$) show that for large R the flow converges to a simple form

$$\mathbf{v} \to \mathbf{v}_0(y, z) + e^{i\alpha x}\mathbf{v}_1(y, z) + e^{-i\alpha x}\mathbf{v}_1^*(y, z) \tag{10}$$

[2] for the y vorticity η with boundary condition $\eta = 0$ or $\partial_y \eta = 0$, or for $\partial_x \omega = (\partial_x^2 + \partial_y^2)v$ with no-slip $v = \partial_y v = 0$ or free-slip $v = \partial_y^2 v = 0$.

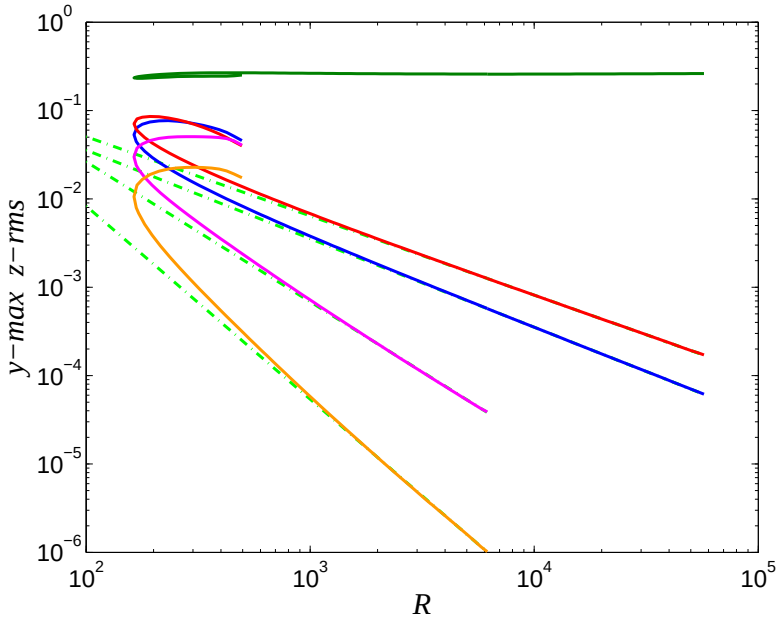

Figure 2: Scalings of the component of the lower branch steady state in plane Couette flow from [24]. The top curve (green) is the amplitude of the streaks $u_0(y,z) - \overline{U}(y) \sim O(1)$ as $R \to \infty$. The 2nd from the top (red) is $w_1 \sim R^{-1}$, the 3rd (blue) is $v_0, w_0 \sim R^{-1}$. The bottom two curves are the higher harmonics $\exp(i2\alpha x)$ (magenta) and $\exp(i3\alpha x)$ (orange) and they converge to zero faster than R^{-1}.

such that $\mathbf{v}_0 = (u_0, v_0, w_0)$ has streaks $u_0(y,z) - \overline{u_0}(y) = O(1)$, but rolls v_0, $w_0 \sim O(R^{-1})$. The x-mode $\mathbf{v}_1(y,z)$ scales *almost* like R^{-1}, see Figure 2. The structure of this lower branch steady state is shown in Figure 3 and the gentle updraft and downdraft supporting $O(1)$ streaks is quite visible together with the critical layer structure of the wave mode $\mathbf{v}_1(y,z)$.

3 SSP model with critical layers

The SSP model [17] discussed in lectures 1 and 5 was intended as an as-simple-as-possible *low Reynolds number* model of the essential process in shear flow that leads to feedback from u onto the shearwise velocity v that creates u through the redistribution of the base shear ($\partial_t u \sim -v\,\partial_y \overline{U} + \cdots$), thereby leading to bifurcation from laminar flow. The model was derived from the Navier-Stokes equations through a Galerkin truncation procedure entirely similar to that needed to derive the Lorenz model of Rayleigh-Bénard convection. The latter is well-known to be physically valid *only* for Rayleigh numbers Ra close to the onset of convection at $Ra_c = 27\pi^4/4$, and the famous chaos of the Lorenz 3-mode model disappears for higher resolution, indeed the chaos is labelled as physically *spurious* [1].[3]

The 3-mode Lorenz model does capture the bifurcation from the conduction state

[3]There are constrained physical systems, *e.g.* the heated fluid loop [9] or the Malkus-Howard water-wheel nicely described in Strogatz's Nonlinear Dynamics and Chaos book, that are governed by the Lorenz equations and do show chaos.

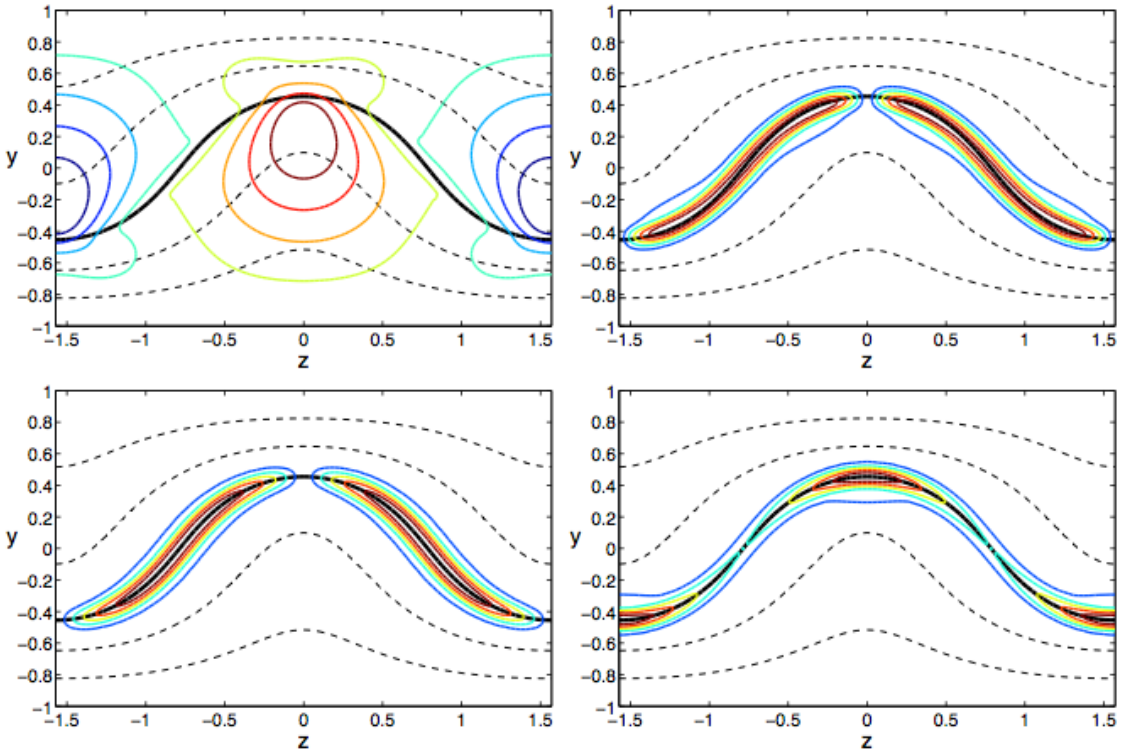

Figure 3: The lower branch plane Couette flow steady state for $\alpha = 1$, $\gamma = 2$, $R = 50\,171$. *Top left:* Contours of $u_0(y, z)$ (dashed, with $u_0 = 0$ thick solid) and $v_0(y, z)$ (color) showing updraft at $z = 0$ and downdraft at $z = \pm\pi/2$. *Top right:* $|u_1(y, z)|$. *Bottom left:* $|v_1(y, z)|$. *Bottom right:* $|w_1(y, z)|$. Note the concentration of u_1, v_1 and w_1 in a $R^{-1/3}$ layer about $u_0 = 0$. From [24].

to a *steady* convection state for $Ra \gtrsim Ra_c$ but for Ra not too far from Ra_c only ($Ra \lesssim 10Ra_c$). The 3-mode model is physically successful for relatively low Ra because the instability is linear and supercritical, *i.e.* it saturates at small amplitudes $\sim (Ra - Ra_c)^{1/2}$ [10]. Likewise the SSP 4-mode model [17] obtained by projection of the Navier-Stokes equations onto a few large scale Fourier modes is expected to be valid only for low R near onset of bifurcated states, but not as accurate as the Lorenz model since the SSP 4-mode model attempts to capture a nonlinear, finite amplitude bifurcation.

Nonetheless, the *lower branch steady states* do appear to result merely from the weakly nonlinear interaction of neutral streaky flow eigenmodes but those streaky flow eigenmodes contain $R^{-1/3}$ critical layers as we have seen. Thus the $R \to \infty$ scalings predicted by the low order model, namely $W \sim R^{-1}$ for the lower branch state (lecture 5 and [17]), may not be correct. Recall that the SSP 4-mode model reads

$$\begin{array}{rcl}
\left(\frac{d}{dt} + \frac{\kappa_m^2}{R}\right) M &=& \frac{\kappa_m^2}{R} \quad -\sigma_u\, UV \qquad\qquad\qquad +\sigma_m\, W^2 \\
\left(\frac{d}{dt} + \frac{\kappa_u^2}{R}\right) U &=& \qquad \sigma_u\, MV \quad -\sigma_w\, W^2 \\
\left(\frac{d}{dt} + \frac{\kappa_v^2}{R}\right) V &=& \qquad\qquad\qquad\quad \sigma_v\, W^2 \\
\left(\frac{d}{dt} + \frac{\kappa_w^2}{R}\right) W &=& \qquad\qquad\quad \sigma_w\, UW \quad -\sigma_v\, VW \quad -\sigma_m\, MW
\end{array} \tag{11}$$

Since W is the amplitude of the only x-dependent mode in the SSP 4-mode model, it is the mode that we should correct for critical layers and its dissipation wavenumber κ_w should be $\kappa_w \sim R^{1/3}$ as $R \to \infty$, as discussed in the previous section. This gives a W decay rate scaling as $\kappa_w^2/R \sim R^{-1/3}$, instead of R^{-1}. The damping wavenumber κ_v for the rolls V also needs to be changed to $R^{1/3}$ in spite of it being x-independent. This is because the rolls are generated through the nonlinear interaction of the streak eigenmode of amplitude W that lives on the critical layer of thickness $\sim R^{-1/3}$ so the dissipation of the rolls occurs at that scale and $\kappa_v \sim R^{1/3}$ also. Likewise the nonlinear interaction coefficients σ_w, σ_v, σ_m scale like $R^{1/3}$ because those originate from the $\mathbf{u}\cdot\boldsymbol{\nabla}\mathbf{u}$ nonlinearity, and when reduced to the V forcing for instance, [17, eqn. (6)], it involves only ∂_y and ∂_z derivatives, *i.e.* derivatives across the warped critical layer of thickness $R^{-1/3}$, so those derivatives scale like $R^{1/3}$. Thus because of the critical layer of the streak eigenmodes we expect

$$\kappa_v, \kappa_w \sim R^{1/3} \qquad \text{and} \quad \sigma_v, \sigma_w, \sigma_m \sim R^{1/3} \tag{12}$$

but κ_m, κ_u and σ_u remain $O(1)$ because the mean shear M and streaks U are x-independent (so no shearing and critical layers for those modes) and they arise from the smooth redistribution of streamwise velocity by the large scale rolls V.

With these modifications, the lower branch steady state would have the $R \to \infty$ scaling U, $M \sim O(1)$ and $V \sim R^{-1}$ but

$$\frac{\kappa_v^2}{R} V = \sigma_v W^2 \;\Rightarrow\; R^{-4/3} \sim R^{1/3} W^2 \;\Rightarrow\; \boxed{W \sim R^{-5/6}} \tag{13}$$

This scaling matches the asymptotic analysis of Hall and Sherwin [4], and the plane Couette numerical results [24], but the asymptotic analysis of the full PDEs is a lot more involved.

4 SSP and Exact Coherent States

4.1 Bifurcation from streaky flow

OK, but how does one find the 3D Navier-Stokes solutions shown in section 2? There are several approaches nowadays, but the original robust approach that worked for plane Couette and plane Poiseuille with both no-slip and free-slip perturbations [18, 19, 20] as well as for pipe flow [2, 25, 11] is based on the self-sustaining process (SSP) shown schematically in Figure 4.

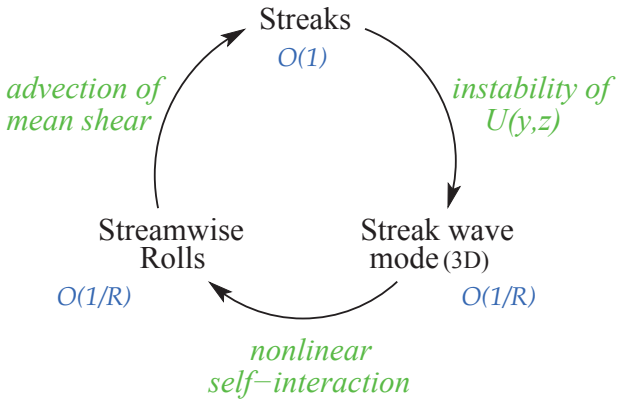

Figure 4: Schematic of the self sustaining process from [17]. Note that the scaling of the 'Streak wave mode' should now be corrected to $R^{-5/6}$.

The SSP was initially conceived as a periodic process where each element would occur in succession: (1) rolls redistribute streamwise velocity to create streaks, (2) streaky flow $U(y,z)$ develops an instability, (3) the nonlinear self-interaction of that instability (essentially an *oblique* vortex roll-up) regenerates the rolls. Indeed, the earliest test of the validity of this process [22, 5] using direct numerical simulations, showed a nearly periodic version of the process and truly time-periodic solutions were later isolated by Kawahara and Kida [6] and Viswanath [15].

But there are also equilibrated versions of the process where the rolls, streaks and streak eigenmode have just the right structure and amplitude to stay in mutually sustained steady or traveling wave equilibrium. The self-sustaining process theory can be used to find 3D steady state or traveling wave solutions of the full Navier-Stokes equations (NSE), *i.e.* the 3D NSE with sufficiently high resolution in all 3 directions. The solutions are represented in terms of Fourier-Chebyshev expansions, Fourier in the x and z directions and Chebyshev in the wall-normal y direction (see [20] for numerical details). The SSP-based procedure to do this [18] is

1. Add $\frac{F}{R^2}$ forcing of rolls $(0, v_0(y,z), w(y,z))$ to NSE $\Rightarrow O(\frac{1}{R})$ rolls, $O(1)$ streaks
2. Find F_c for *onset* of instability of $[u_0, v_0, w_0](y,z)$ for given α (or α_c for given F).
3. Use W (amp of $e^{i\alpha x}$ mode) as control parameter and continue to $F = 0$ (*Subcritical* bifurcation thanks to nonlinear feedback from wave mode onto rolls).

The parameter F is $O(1)$ and R is the Reynolds number [17, 18, 20]. This procedure is illustrated in Figures 5, 6 and 7 for free-slip plane Couette flow ('FFC' = 'Free-Free

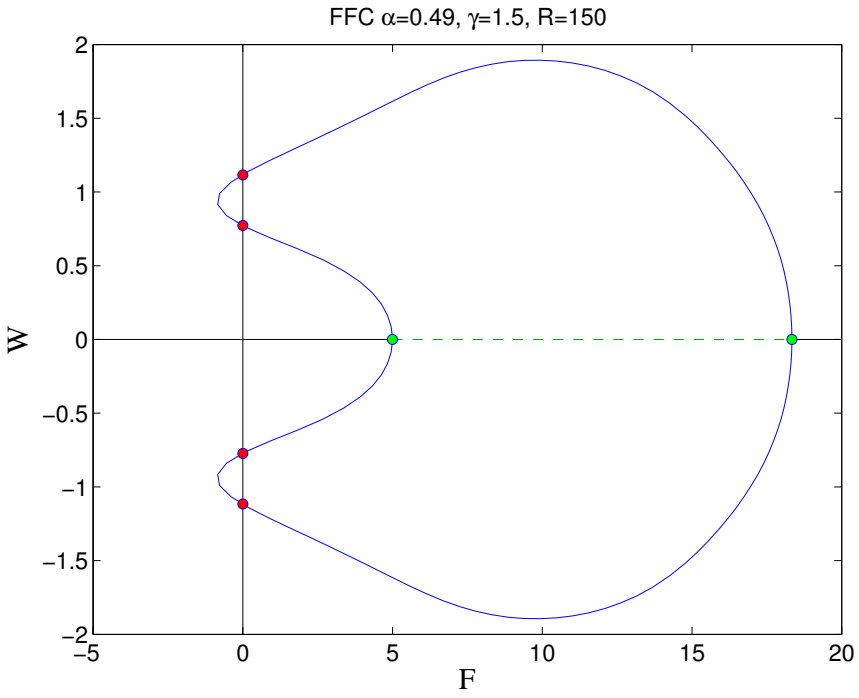

Figure 5: Bifurcation diagram for Free-Free Plane Couette Flow with $\alpha \approx 0.49$, $\gamma = 1.5$, $R = 150$, fixed. $F = W = 0$ is the laminar flow $U = y$. $W = 0$ corresponds to x-independent streaky flow with rolls and streaks when $F \neq 0$. The green markers at $W = 0$, $F = 5, 18.3$ are the streaky flow bifurcation points and the streaky flow is unstable between those markers (dashed line). The red markers at $F = 0$ indicate the self-sustained 3D steady states. Since W is the amplitude of the $e^{i\alpha x}$ mode, a change of sign of W corresponds to a half-period shift in x. This is for well-resolved spectral calculations of the full Navier-Stokes equations *not* the low-order model, although the low-order model has similar behavior.

Couette') where it is particularly clean since the roll forcing has a simple form to yield the $v_0(y,z) = (F/R)\cos\beta y \ \cos\gamma z$ with $\beta = \pi/2$ from lecture 5. Here $F_c = 5$ for $\alpha \approx 0.49$ and $\gamma = 1.5$ at $R = 150$. $F = 0$, $W = 0$ is the laminar flow $u = y$ with $u = 0$ at $y = 0$ (the green surfaces in Figures 6, 7, the yellow surface is $u = -0.5$). For $F \neq 0$, we are forcing simple streamwise rolls seen as the red and blue tubes in Fig. 6 that redistribute the streamwise velocity u, warping the isosurfaces $u = constant$, to create a 2D streaky flow. Increasing F beyond a critical value F_c leads to an unstable streaky flow, although when F becomes too big, the rolls stir up the flow so much that the mean shear and streaks are wiped out and the streaky flow regains stability. This streaky flow for $\alpha = 0.49$, $\gamma = 1.5$, $R = 150$ is unstable for $5 < F < 18.3$ (*i.e.* fixed geometry, although we usually fix F and find the band of unstable α). Taking W, the normalized amplitude of the $e^{i\alpha x}$ mode, as the control parameter and increasing from $W = 0$ leads to the sequence of 3D steady states shown in figures 6 and 7 yielding to self-sustained states with no roll forcing ($F = 0$).

This procedure can be used in other flows: Rigid-Rigid Couette (*i.e.* no-slip at both walls), Rigid-Free Couette, Rigid-Free Poiseuille, Rigid-Rigid Poiseuille as well as in no-slip pipe flow [2, 25, 11] and duct flow (Kawahara *et al.*).

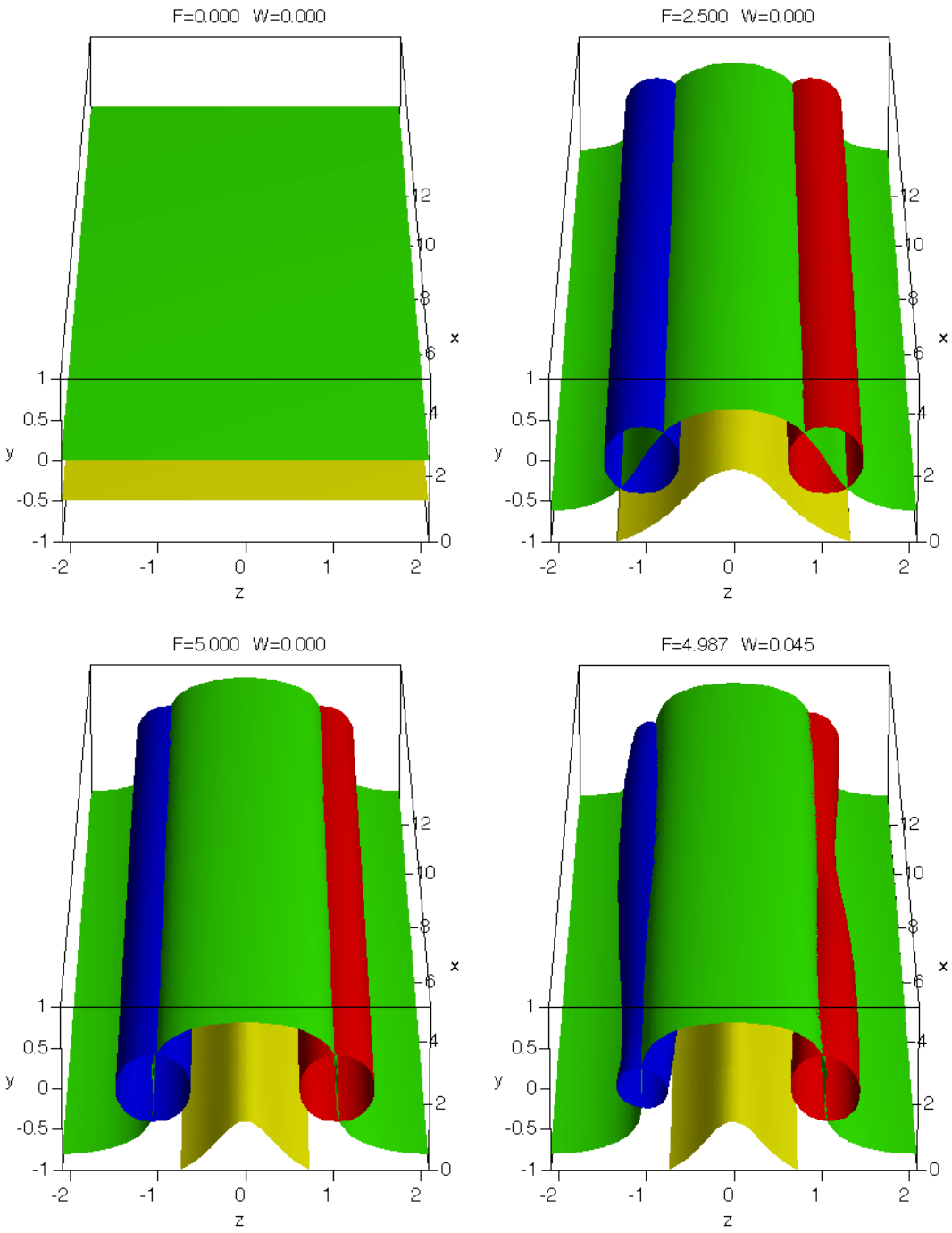

Figure 6: SSP construction of exact coherent states for Free-Free Plane Couette Flow. The green surfaces are $u = 0$, gold is $u = -0.5$. Red and blue correspond to positive and negative streamwise vorticity ω_x, respectively (80% of max). F is the normalized roll $v_0(y, z)$ amplitude and W is the normalized $e^{i\alpha x}$ streaky mode amplitude. First we increase F with $W = 0$ until the 2D streaky flow is unstable (bottom left), then we start increasing W with F free.

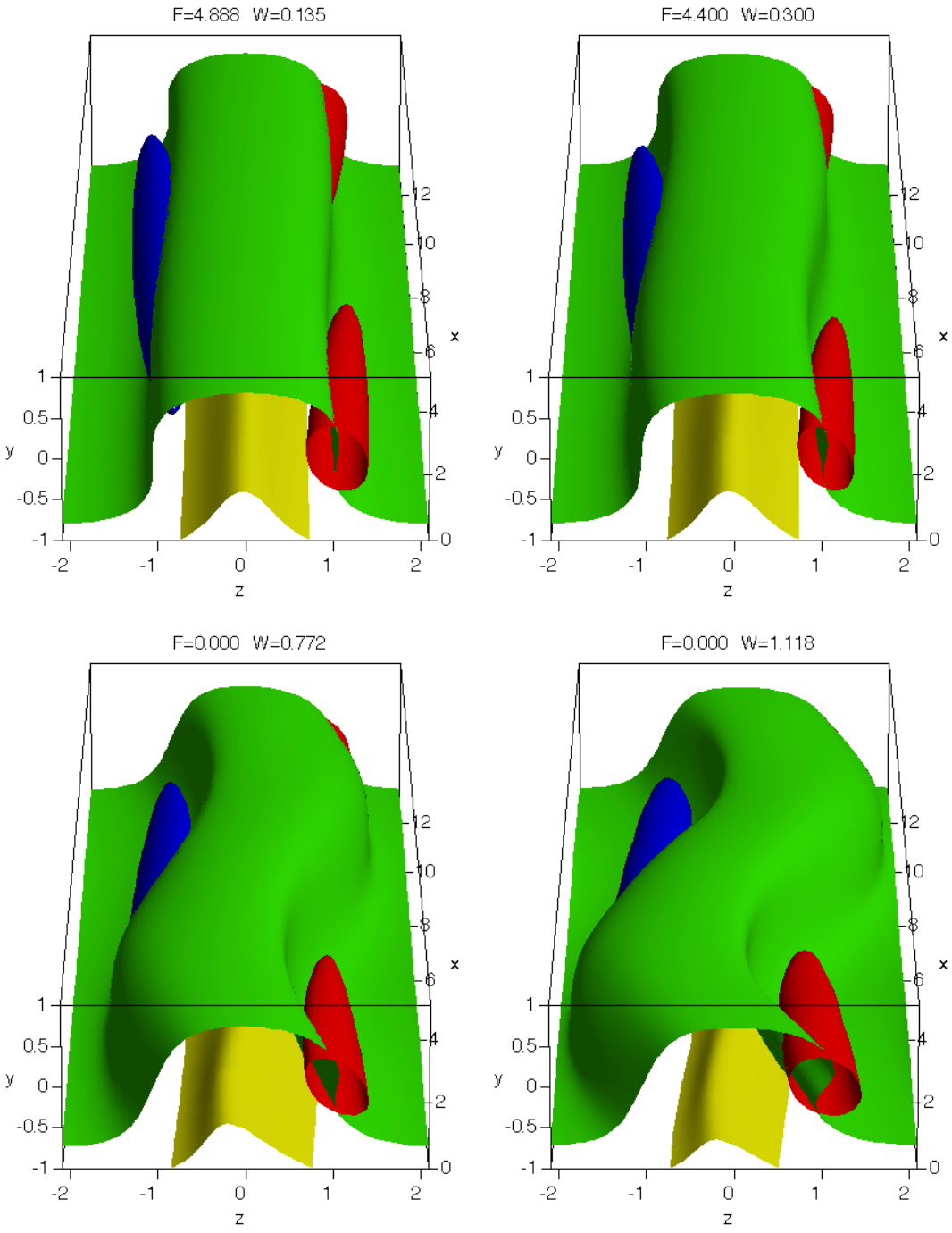

Figure 7: Continued from Fig. 6, we keep on increasing W and obtain a lower branch self-sustained steady state when $F = 0$ (bottom left) and an upper branch (bottom right). These are the upper two red markers in the bifurcation diagram Fig. 5.

4.2 Homotopy of exact coherent states

The solutions can also be easily 'deformed' into one another. For instance one can perform the homotopy from *Free-Free Couette* to *Rigid-Free Poiseuille*, this is a Newton continuation of the steady state Couette solutions to *traveling wave* Poiseuille solutions in a half-channel with no-slip at the bottom wall at $y = -1$ and free-slip at the centerline at $y = 1$. This is the homotopy

$$\begin{aligned} U_L(y) &= y + \mu\left(\frac{1}{6} - \frac{y^2}{2}\right) \\ (1-\mu)\frac{\partial u}{\partial y} + \mu\, u &= 0 \qquad \text{at} \qquad y = -1 \end{aligned} \tag{14}$$

and similarly for w at the wall, with $\mu = 0 \to 1$ to go from Couette with free slip at both walls to Poiseuille $U_L(y) = 1/6 + y - y^2/12$ with no-slip at the bottom wall, where $U_L(y)$ is the laminar flow and Poiseuille is normalized to be nearest to Couette. If this homotopy is performed at fixed W (amp of $e^{i\alpha x}$ mode) then R becomes the free parameter, since we are now only interested in self-sustained 3D states with no external roll forcing $F = 0$ (Figure 8).

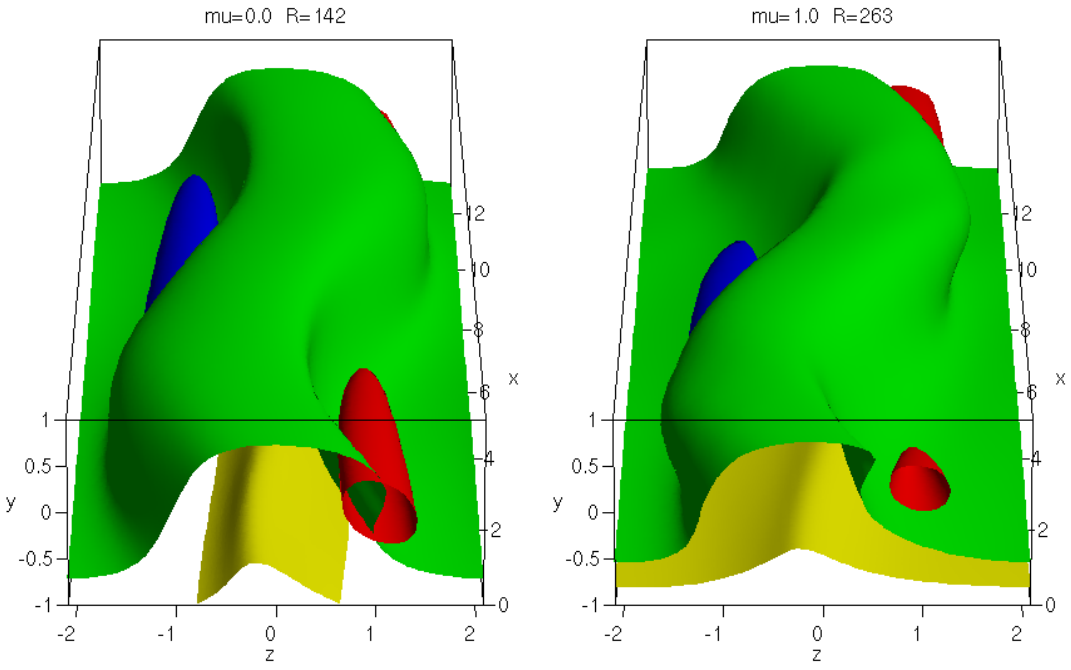

Figure 8: Homotopy (14) from free-free Couette $\mu = 0$ (left) to Rigid-free Poiseuille at $\mu = 1$ (right) [18, 19]. The gold $u = -0.5$ isosurface cannot be swept away with no-slip at $y = -1$ (right). The green isosurface on the right is $u - c = 0$ where c is the wave speed.

By 'homotopy' we mean to emphasize the very similar ('homo') shape ('topos') of the solutions in the various flows, *e.g.* free-slip Couette and no-slip Poiseuille, and the 'homotopy' procedure consists of a smooth deformation of one solution into the other. In contrast, we used bifurcation from streaky flow to construct the solution from scratch

and that is not smooth since it involves a bifurcation (sect. 4.1). In the literature, authors often refer to the latter as 'homotopy' as well, but we do not.

4.3 'Optimum' channel Traveling Wave

Once a self-sustained 3D steady state or traveling wave has been found, it is interesting to find its lowest onset Reynolds number. To do so we need to optimize the 3D solutions over the fundamental wavenumbers α and γ, *i.e.* over the wavelengths L_x and L_z in order to minimize the Reynolds number. This was done for a variety of flows, including Rigid-Rigid Couette where onset $R \approx 127.7$ and Rigid-Free Poiseuille where onset $R \approx 977$ (based on the laminar centerline velocity and the wall to centerline distance to compare to 5772 for onset of the weak 2D viscous no-slip instability). Note that there is a factor of 4 difference arising just from the different definitions of R in plane Couette and Poiseuille.

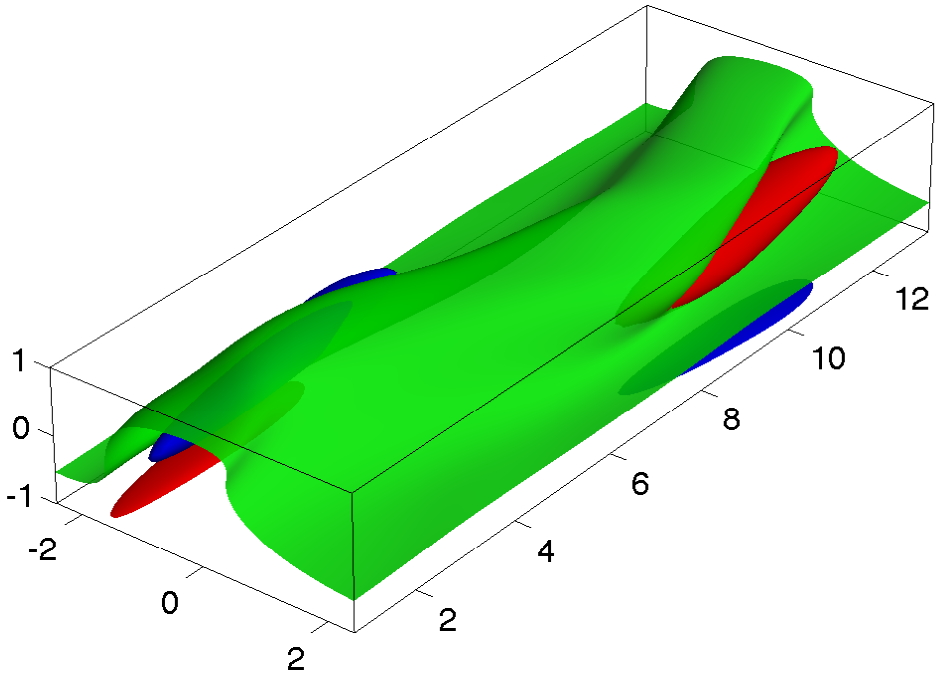

Figure 9: Channel flow traveling wave at onset Reynolds number $R_\tau \approx 44$ for $L_x^+ \approx 274$ and $L_z^+ \approx 105$ in wall units. This corresponds to a pressure gradient based Reynolds number (*i.e.* laminar centerline velocity and wall to centerline distance) of 977 [20]. R_τ is based on the friction velocity $u_\tau = \sqrt{\tau_w}$ and the wall to centerline distance. Wall or 'plus' units are based on ν/u_τ. Each vortex (red and blue isosurfaces) has a shear layer of opposite sign ω_x at the wall below it. The green isosurface is $u - c = 0$ where c is the traveling wave speed.

One remarkable result of this optimization is that the length scales for minimum

onset Reynolds number turn out to be almost identical to the length scales that had long been observed for *coherent structures* in the near-wall region of turbulent channel flows, namely $L_x^+ \approx 300$, $L_y^+ \approx 50$ and $L_z^+ \approx 100$, the latter corresponding to the well-known 100+ streak spacing. This fits with the idea that those scales are the smallest scales for the self-sustaining process and the streak spacing is essentially an onset Reynolds number [16]. The structure of the traveling wave is also remarkably similar to the educed structure of near wall momentum transporting flows shown in Figure 10. Those observed structures consists of wavy low speed streaks flanked by staggered counterrotating quasi-streamwise vortices, exactly like the 3D traveling waves, hence the name of *exact coherent states* for the latter [19].

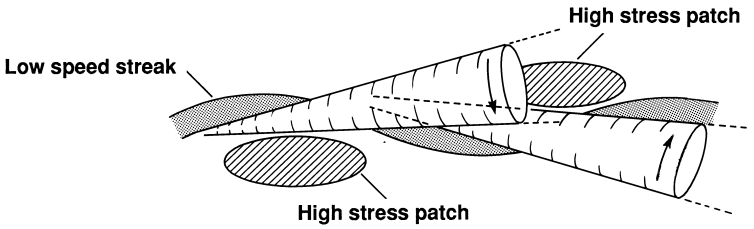

Figure 10: Near-wall coherent structure educed from turbulent channel data by Derek Stretch (1990) [14]. Note the wavy streak as the wavy green isosurface in Fig. 9 and the counterrotating quasi-streamwise vortices as the red and blue isosurfaces in Fig. 9, and the earlier Couette solutions in Fig. 7.

5 Turbulence: onset and structure in state space

We saw in sect. 4.1 how the exact coherent states — 3D steady states and traveling wave solutions of the Navier-Stokes equations — can be constructed by bifurcation from streaky flow in the (F, W) parameter space for fixed R, α, γ (Fig. 5). For fixed $F = 0$ these solutions arise from *saddle-node* bifurcations, also known as *out-of-the-blue-sky* bifurcations, in the (R, W) parameter plane, as shown in Figure 11. Although the drag of the upper branches grows quickly with Reynolds number, at least initially (we expect fixed (α, γ) solutions to eventually saturate), the lower branch solution quickly asymptotes to a constant *larger than the laminar drag.* These computations have been pushed to $R \approx 60\,000$ and the lower branch drag appears constant, consistent with Fig. 2 where the solution asymptotes to O(1) streaks. This suggest that these solutions never bifurcate from the laminar flow, not even at $R \to \infty$.

But all these upper and lower branches are *unstable from onset*, how then could they be relevant? We have already seen that their structure and length scales (*e.g.* the 100+ streak spacing) match very well with the observed near-wall coherent structures in turbulent shear flows, and the latter are clearly unstable, yet they are statistically ever present and control the momentum transport. Figure 12 provides other evidence of the relevance of unstable coherent states to turbulent flows that appear to oscillate around the upper branches, suggesting that the upper branch is a good first approximation to the statistics of turbulent flows such as drag, energy dissipation, mean flows, ...

The lower branch on the other hand has the remarkable property of having only one unstable direction, at least in plane Couette flow except close to the nose of the bifurcation curve [24]. Starting in the unstable direction either leads quickly to turbulent flow, or in the opposite direction leads quickly back to laminar flow as shown in Figure 13.

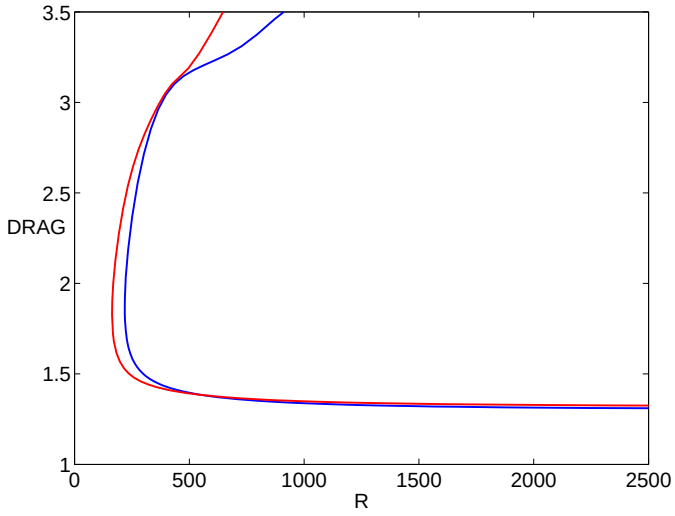

Figure 11: Rigid-rigid Couette bifurcation diagram for 3D steady states for $(\alpha, \gamma) = (1, 2)$ (red) and (1.14,2.5) (blue). Drag versus Reynolds number. Drag is non-dimensionalized by the laminar drag so this is a Nusselt number, $\tau_w/(\nu U/h)$ and Drag=1 is the laminar flow. The upper branch drag increases rapidly with R but the lower branch quickly asymptotes to a constant > 1. The solutions arise *out-of-the-blue-sky* but do not bifurcate from the laminar flow.

This suggests that the lower branch is the backbone of the laminar-turbulent boundary that would be the *stable manifold* of the lower branch. Further calculations by us and others have confirmed this role of the lower branch [12].

Figure 14 is an old cartoon (APS DFD 2001, [19], [21]) sketching how these exact coherent states and their stable and unstable manifold structure the state space. Gibson, Cvitanović and Halcrow [3] have produced a beautiful picture of the state space of plane Couette flow for given fundamental wavenumber (α, γ) and Reynolds number $R = 400$ that shows the role of the coherent states and their unstable manifolds in guiding the turbulent dynamics. Kawahara, Uhlmann and van Veen explore the relevance of invariant solutions for fully developed turbulent flows [7].

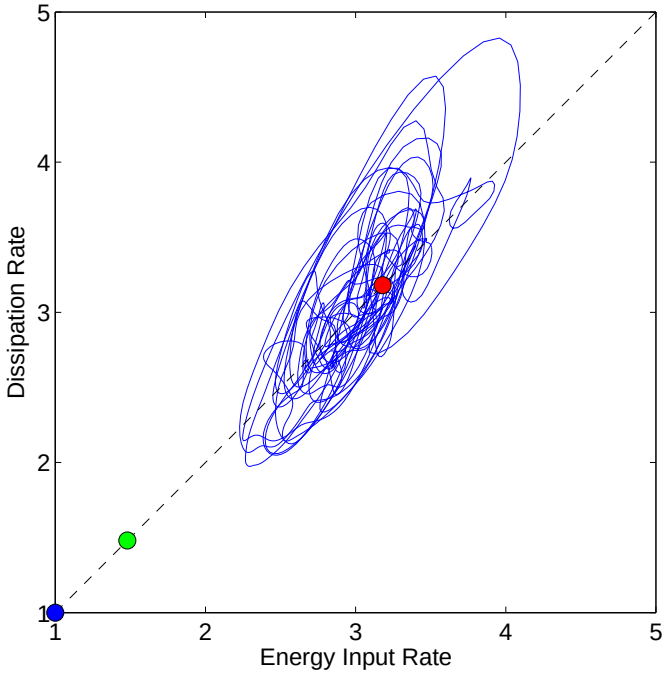

Figure 12: Rigid-rigid Couette 3D steady states for $(\alpha, \gamma) = (0.95, 1.67)$ in the total energy input rate $\tau_w U/h$ versus total energy dissipation rate $\mathcal{E}$ (lecture 2), normalized by laminar values so blue marker is laminar flow at (1,1). Green marker is lower branch, red marker is upper branch. The blue orbit is a DNS of turbulent flow for 2000 h/U time units for $(\alpha, \gamma) = (1.14, 1.67)$. Turbulent orbit was computed by Jue Wang using John Gibson's Channelflow code [24].

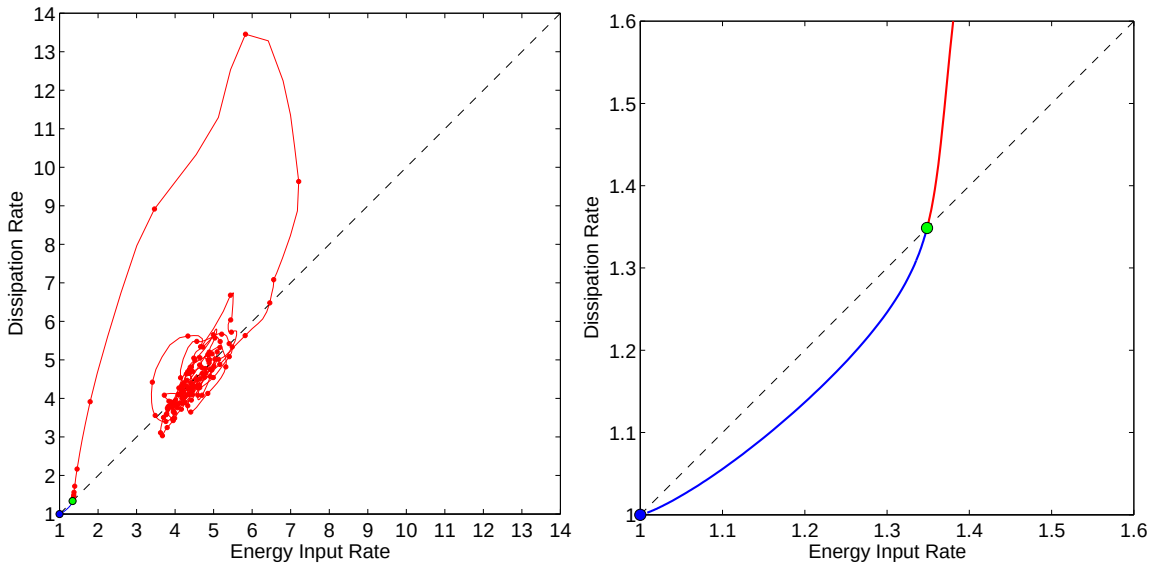

Figure 13: Rigid-rigid Couette for $(\alpha, \gamma) = (1, 2)$ at $R = 1000$. Starting on the positive (say) side of the lower branch unstable direction quickly leads to a turbulent flow that oscillates about upper branches (left). Starting on the opposite side quickly leads to a slow, reverse SSP, decay back to laminar. That is, the flow first loses its x dependence, then the rolls and streaks slowly decay back to laminar flow (right). Note the different scales. The dots on the red curve mark equal time intervals to show speed along the curve.

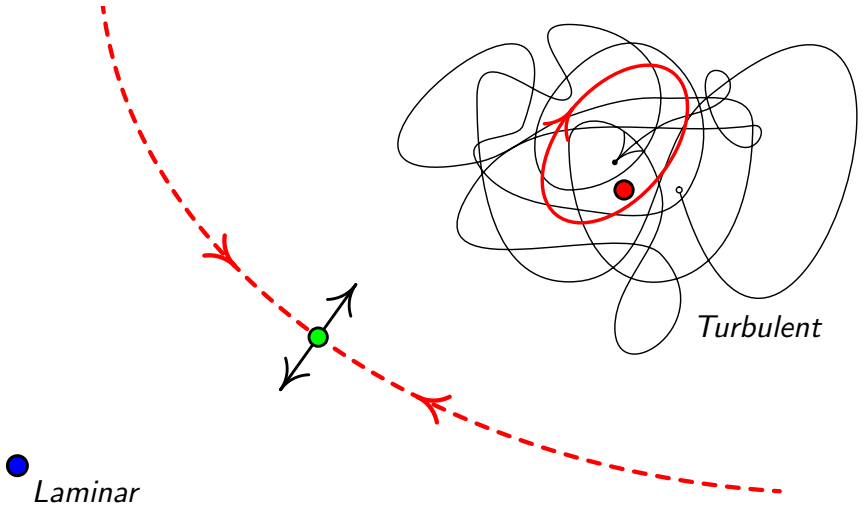

Figure 14: Schematic of the state space and role of the unstable exact coherent states. Laminar flow (blue) is stable for all R. Lower branch is the backbone of the laminar-turbulent boundary which is the stable manifold (red dashed) of the lower branch (green marker). The turbulent flow is an aperiodic oscillation about upper branches (red marker). There exists also unstable periodic orbits (red curve), that form the skeleton of the turbulent attractor.

5.1 Conclusion

These six lectures have been a quick and necessarily incomplete overview of the problem of turbulence onset and structure in basic flows such as flows in pipes and channels. The scientific study of this basic fluid dynamics problem started with the experiments of Reynolds and the analyses of Rayleigh in the 1880s and has been an active field of study ever since, splitting into several distinct directions such as stability theory, turbulence modeling and statistical theories of turbulence.

Linear stability theory of shear flows does not explain onset of turbulence but has many technical and physical peculiarities such as critical layers and (weak) instability arising from viscosity in channel but not in pipe, in pressure-driven but not wall-driven flows, yet turbulence in all these different flows is quite similar. Statistical theories have focused largely on homogeneous isotropic turbulence and disconnected drag from energy dissipation. The Kolmogorov picture of turbulence with its energy cascade concept and $k^{-5/3}$ energy spectrum is compelling, but has little if anything to say about momentum transport or heat flux in realizable wall-bounded flows. Numerical simulations and modern experimental visualization techniques such as PIV (particle image velocimetry) have revealed a myriad of coherent structures and a major challenge has been to decide how to identify and classify these observed structures and their interconnections, and figure out how to introduce them in models and theories.

Our work on exact coherent states reconnects turbulence onset to developed turbulence with its observed and educed coherent structures. The 100+ streak spacing of near-wall coherent structures in fully developed turbulent shear flows is closely related to, if not identical with, the critical Reynolds number for turbulence onset [16], [20]. In a little more than a decade, we have gone from the two well-known states of fluid flow, *laminar* and *turbulent*, to the discovery of a multitude of intermediate states, *unstable exact coherent states*. These states can be steady states or more generally traveling waves in plane Couette, Poiseuille, pipe and duct flows as well as time periodic solutions. The latter have been found mostly in plane Couette flow so far, by Kawahara and Kida [6], Viswanath [15] and many unpublished states found by John Gibson (but posted on his web page). Schneider, Gibson and Burke [13] have found spanwise localized states that bifurcate from the lower branch states close to the 'nose' of the saddle-node bifurcation. This bifurcation is directly connected to the Hopf bifurcation that was known to occur along the lower branch as we approached the saddle-node bifurcation [23], [24], and to the instability of the upper branch (the node) at onset.

Our cartoon (Fig. 14) is now too simplistic, there are many lower branches and upper branches, even snakes and ladders [13], and Eckhardt and co-workers have shown that there are more complex types of *'edge states'* on the laminar-turbulent boundary than mere traveling waves. Lebovitz [8] uses low order models to explore features of the laminar-turbulent boundary and shows that the 'edge' may not be a laminar-turbulent boundary but an invariant set separating the basin of attraction of the laminar state in two parts. We have discovered the unstable coherent scaffold of turbulent flows and, not surprisingly, it is rich and complex.

References

[1] J. H. Curry, J. R. Herring, J. Loncaric, and S. A. Orszag, *Order and disorder in two- and three-dimensional Bénard convection*, Journal of Fluid Mechanics, 147 (1984), pp. 1–38.

[2] H. Faisst and B. Eckhardt, *Traveling waves in pipe flow*, Phys. Rev. Lett., 91 (2003), p. 224502.

[3] J. F. Gibson, J. Halcrow, and P. Cvitanović, *Visualizing the geometry of state space in plane Couette flow*, Journal of Fluid Mechanics, 611 (2008), pp. 107–130.

[4] P. Hall and S. Sherwin, *Streamwise vortices in shear flows: harbingers of transition and the skeleton of coherent structures*, Journal of Fluid Mechanics, 661 (2010), pp. 178–205.

[5] J. Hamilton, J. Kim, and F. Waleffe, *Regeneration mechanisms of near-wall turbulence structures*, J. Fluid Mech., 287 (1995), pp. 317–348.

[6] G. Kawahara and S. Kida, *Periodic motion embedded in Plane Couette turbulence: regeneration cycle and burst*, J. Fluid Mech., 449 (2001), pp. 291–300.

[7] G. Kawahara, M. Uhlmann, and L. van Veen, *The significance of simple invariant solutions in turbulent flows*, Annu. Rev. Fluid Mech. 44 (2012), pp. 203–225.

[8] N. R. Lebovitz, *Boundary collapse in models of shear-flow transition*, Communications in Nonlinear Science and Numerical Simulation, 17 (2012), pp. 2095 – 2100.

[9] W. V. R. Malkus, *Non-periodic convection at high and low Prandtl number*, Mém. Soc. R. Sci. Liège, 4 (1972), pp. 125–128.

[10] W. V. R. Malkus and G. Veronis, *Finite amplitude cellular convection*, Journal of Fluid Mechanics, 4 (1958), pp. 225–260.

[11] C. C. T. Pringle and R. R. Kerswell, *Asymmetric, helical, and mirror-symmetric traveling waves in pipe flow*, Physical Review Letters, 99 (2007), p. 074502.

[12] T. Schneider, J. Gibson, M. Lagha, F. De Lillo, and B. Eckhardt, *Laminar-turbulent boundary in plane Couette flow*, Phys. Rev. E, 78 (2008), p. 037301.

[13] T. M. Schneider, J. F. Gibson, and J. Burke, *Snakes and ladders: Localized solutions of plane couette flow*, Phys. Rev. Lett., 104 (2010), p. 104501.

[14] D. Stretch, *Automated pattern eduction from turbulent flow diagnostics*, in Annual Research Briefs, Center for Turbulence Research, Stanford U., 1990, pp. 145–157.

[15] D. Viswanath, *Recurrent motions within plane Couette turbulence*, J. Fluid Mech., 580 (2007), pp. 339–358.

[16] F. Waleffe, *Proposal for a self-sustaining process in shear flows*, Working paper, available at `www.math.wisc.edu/~waleffe/ECS/sspctr90.pdf`, (1990).

[17] ——, *On a self-sustaining process in shear flows*, Phys. Fluids, 9 (1997), pp. 883–900.

[18] ——, *Three-dimensional coherent states in plane shear flows*, Phys. Rev. Lett., 81 (1998), pp. 4140–4148.

[19] ——, *Exact coherent structures in channel flow*, J. Fluid Mech., 435 (2001), pp. 93–102.

[20] ——, *Homotopy of exact coherent structures in plane shear flows*, Phys. Fluids, 15 (2003), pp. 1517–1543.

[21] ——, *Exact coherent structures in turbulent shear flows*, in Turbulence and Interactions: Keynote Lectures of the TI 2006 Conference, M. Deville, T.-H. Le, and P. Sagaut, eds., Springer, 2009, pp. 139–158.

[22] F. Waleffe, J. Kim, and J. Hamilton, *On the origin of streaks in turbulent shear flows*, in Turbulent Shear Flows 8: selected papers from the Eighth International Symposium on Turbulent Shear Flows, Munich, Germany, Sept. 9-11, 1991, F. Durst, R. Friedrich, B. Launder, F. Schmidt, U. Schumann, and J. Whitelaw, eds., Springer-Verlag, Berlin, 1993, pp. 37–49.

[23] J. Wang, *On lower branch Exact coherent structures in Turbulent shear flows*, Ph.D. Thesis, University of Wisconsin-Madison, 2007.

[24] J. Wang, J. Gibson, and F. Waleffe, *Lower branch coherent states in shear flows: transition and control*, Phys. Rev. Lett., 98 (2007), p. 204501.

[25] H. Wedin and R. Kerswell, *Exact coherent structures in pipe flow*, J. Fluid Mech., 508 (2004), pp. 333–371.